SIMULATION STRATEGY OF A NOVEL SCROLL EXPANDER USING REMESH TECHNIQUE

Filipi Martins Fernandes Silva, filipimfs@gmail.com[1]
Fernando de Oliveira, fernandovo@yahoo.com.br[1]
Paulo Eduardo Batista de Mello, pmello@fei.edu.br[1]

[1]Centro Universitário da FEI - Av. Humberto Castelo Branco, 3972 - São Bernardo do Campo - São Paulo - Brazil

Abstract: *Compressed air energy storage (CAES) and organic Rankine cycle (ORC) are highly influenced by the expander isentropic efficiency. Scroll expanders are indicated for low power cycles, usually lower than 10 kW. Those expanders have their isentropic efficiency decreased by internal leakage, as shown on previous works. We present herein a transient 2D simulation of a scroll expander using the remesh technique that quantifies the internal leakage. Simulation strategies are discussed on this paper, including the remesh process, since this may lead to inefficiency. The results are compared to the model described by Mendoza* et al. *(2014) applied to our novel scroll expander.*
Keywords: *Scroll expander, CAES, ORC, internal leakage, CFD*

1. INTRODUCTION

The use of scroll geometry is well established for the design of compressors and vacuum pumps. However, its use as expander to produce power is more recent, with the first proposals 20 years ago, with promising results obtained by Zanelli and Favrat (1994). In this earlier study, Zanelli and Favrat (1994) propose the use of isentropic efficiency and filling factor parameters to characterize the performance of the machine. Another example of experiment with scroll expanders may be found in Yanagisawa *et al.* (2001). The isentropic efficiency obtained in these first attempts to use scroll expanders ranged between 60% to 65%.

Considering the possible use of scroll expanders in the implementation of ORC (organic Rankine cycle) and CAES (compressed air energy storage), a significant number of recent works have been done about the subject. Declaye *et al.* (2013) and Mendoza *et al.* (2014) report the measurement of maximum isentropic efficiency of 75.7% and 61% in its experimental tests, respectively.

The prediction of the performance of a scroll expander can be conducted with the model proposed by Lemort *et al.* (2009). The model was exhaustively tested against experiments presenting very good agreement. The model permits to map the main losses presented in the machine: under-expansion or over-expansion and internal leakages. Less relevant losses are pressure drop in the inlet, friction and heat transfer. In order to use the model, a set of parameters must be adjusted from experiments. This limits its use to existing expanders for each experimental data is available.

The use of CFD (computational fluid dynamics) for the simulation of scroll expanders is recent. A good review is presented in Song *et al.* (2015), where the authors select 9 relevant papers on the last 26 years about numeric simulation of scroll machines; three of them are 2D. The author also states that due to the motion and the complex geometry of this machine, the simulations are still in an early stage.

Song *et al.* (2013) adapted a scroll compressor to work as a scroll expander and performed a 3D transient simulation using dynamic mesh and R245fa as working fluid. The authors presented results for pressure, temperature and velocity distributions and the behaviour of the torque, power and mass flux.

In this work we present a simulation strategy for the CFD simulation of scroll expanders. Our study is focused on the geometry of a novel scroll expander prototype for which experimental data was obtained by Fanti *et al.* (2016). The simulation uses a 2D geometry and, despite its apparent simplicity, the results are reasonably in good agreement with the analytical model predictions and experimental measurements.

2. GEOMETRY

The geometry selected for the simulations is the same used to construct the prototype proposed by Fanti *et al.* (2016) for which experimental measurements are available. The equations that determine the involute of circle are described in details by Blunier *et al.* (2009). We constructed the geometry of the walls using a CAD program and imported the resultant files to Ansys Workbench for grid generation.

The main parameters that describe the walls are the radius of the involute basic circle r_b and many angles that define the start and ending points of the different curves. The parameters and the values used to construct the curves are summarized in Tab. 1.

The wall curves for the external and internal walls of the fixed scroll may be described by 1 and 2.

$$\mathbf{S}_{fe}(\varphi) = r_b\mathbf{t}(\varphi) - r_b\left(\varphi - \varphi_{e0}\right)\mathbf{n}(\varphi) \quad \forall\varphi \in [\varphi_{es}, \varphi_{max}] \tag{1}$$

$$\mathbf{S}_{fi}(\varphi) = r_b\mathbf{t}(\varphi) - r_b\left(\varphi - \varphi_{i0}\right)\mathbf{n}(\varphi) \quad \forall\varphi \in [\varphi_{is}, \varphi_{max}] \tag{2}$$

In 1 and 2 an orthonormal frame is used, defined by a tangent vector and an unit normal vector, respectively defined by 3 and 4.

$$\mathbf{t}(\varphi) = (cos\varphi, sin\varphi) \tag{3}$$

$$\mathbf{n}(\varphi) = (-sin\varphi, cos\varphi) \tag{4}$$

The scroll walls have constant thickness, determined by 5.

$$e = r_b\left(\varphi_{i0} - \varphi_{e0}\right) \tag{5}$$

Following the approach proposed by Blunier *et al.* (2009), we define the geometry of the orbiting scroll wall from the fixed one offsetted by π. The orbiting angle θ appears in 6 and 7 defining the relative position between fixed and moving scroll walls.

$$\mathbf{S}_{me}(\varphi) = -\mathbf{S}_{fe}(\varphi) - r_o\mathbf{n}(\theta) \tag{6}$$

$$\mathbf{S}_{mi}(\varphi) = -\mathbf{S}_{fi}(\varphi) - r_o\mathbf{n}(\theta) \tag{7}$$

The use of the nominal orbiting radius r_o, given by 8 would result in walls that touch each other. To avoid this condition, the orbiting radius is reduced, creating a gap between the walls and a leakage path.

$$r_o = r_b\left(\varphi_{e0} - \varphi i0 + \pi\right) \tag{8}$$

The inclusion of the gap between the walls in the simulation is essential to adequately predict the behavior of the machine. The flank internal leakages is caused by this gap between the walls. Of course, the device is manufactured with this gap as low as possible to decrease this leakage. Fanti *et al.* (2016) used 200 μm as initial flank gap and intends to investigate the influence of the gap over expander performance.

Table 1: **Parameters that define the geometry of the walls**

Parameter	Symbol	Value
Radius of the involute basic circle	r_b	23/2 π mm
Wall thickness	e	5 mm
Initial angle of external involute	φ_{e0}	$-e/2r_b$
Initial angle of internal involute	φ_{i0}	$e/2r_b$
Involute final angle	φ_{max}	15/2 π
External starting angle	φ_{es}	π/2
Internal starting angle	φ_{is}	π/2
Nominal orbiting radius	r_o	6.5 mm

3. NUMERICAL MODEL

The simulation is a 2D transient turbulent flow without heat transfer in the walls. The second-order backward Euler scheme implemented in CFX was used for the discretization of the transient term, while convection terms were discretized with the high order scheme. The air flow was modelled considering ideal gas properties. Turbulence model SST k-ω was chosen and boundary conditions were specified according to Fig. 1.

Total pressure and total temperature was imposed at the scroll inlet; pressure was imposed in the outlet (see Tab. 2 for values). The rotation speed was constant and equal to 2,700 rpm. The moving scroll wall advanced by 0.125°per time step. These parameters determine the time step value and were obtained after tests with the solver, resulting in good convergence.

Table 2: **Inlet and outlet boundary conditions**

Inlet total pressure	3.8 bar (abs)
Inlet total temperature	300 K
Outlet pressure	1.0 bar (abs)

The simulation ran for 10 complete revolutions in order to guarantee a stable behavior: repeatable results between two revolutions. During the first revolution the pressure imposed at inlet boundary condition is raised in a linear form to avoid divergence. The inlet pressure is maintained constant after this first revolution.

To save computational time the mesh chosen was a quasi-2D unstructured with only 5 mm of height (Fig. 2). The convergence criteria for mass, momentum and turbulence variables was residual RMS value lower than 10^{-4}.

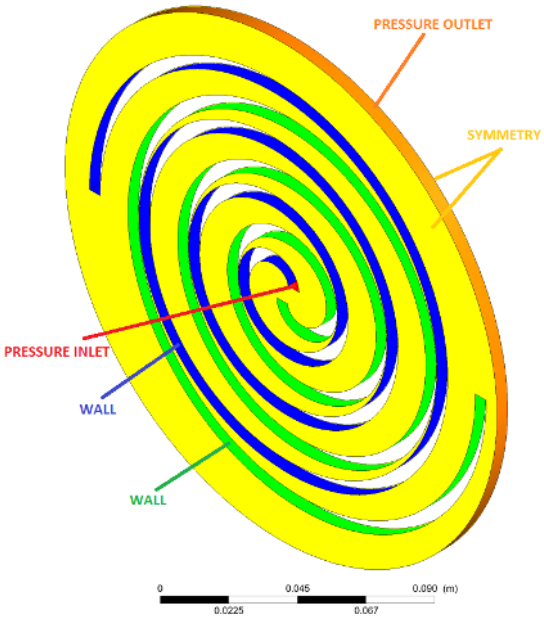

Figure 1: **Location of boundary conditions**

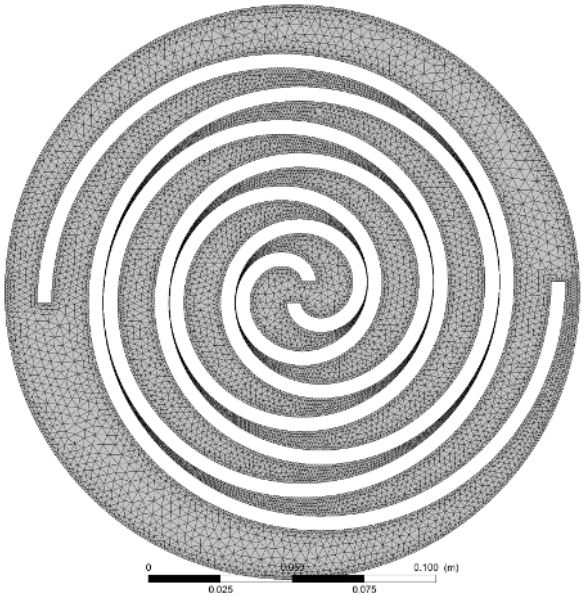

Figure 2: **2D mesh used at θ = 0°**

4. STRATEGY USED TO PERFORM THE REMESH

Ansys CFX provide routines for implementation of mesh deformation. However, there is a limitation due to mesh quality: if any element gets a negative volume, the solution is going to stop due to numerical error. Remesh technique works generating a new mesh when the actual mesh gets too deformed and either does not describe correctly the geometry (e.g. a volume passes through a wall) or an element gets a negative volume that leads to numerical error.

The common remesh strategy works stopping the solver when a stopping criteria specified by the user is reached. At this point the mesh generator is called, generates a new mesh and restart the simulation from where it stopped, interpolating the results from the last deformed mesh to the new undeformed one. This solution is pretty slow, what increases the computational time even for a two-dimensional simulation.

To solve this problem we have generated meshes from 0° to 359° and developed a stopping criteria that calls the correct mesh for the correct angular position when the mesh gets too deformed. This is possible by monitoring the orthogonality from all mesh elements and checking the minimum value (see Fig. 3); if this value gets smaller than 27° and there is a mesh for the current angle, the remesh routine is called and the mesh is replaced by a new one with best quality. This procedure is illustrated on Fig. 4. In our simulations the remeshing occurred 116 times per revolution.

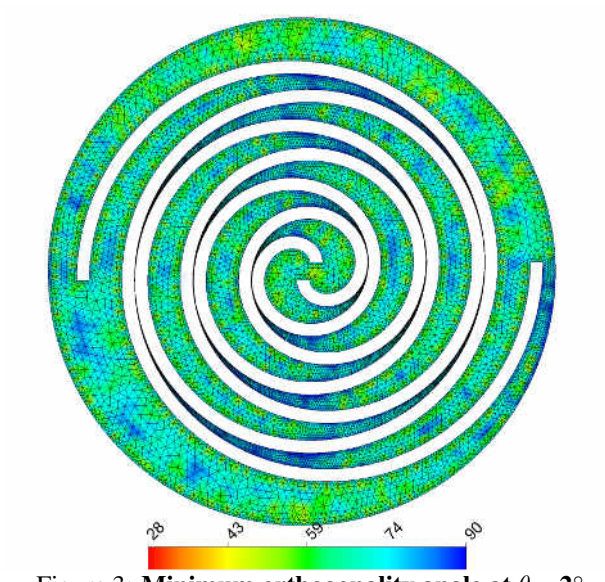

Figure 3: **Minimum orthogonality angle at θ = 2°**

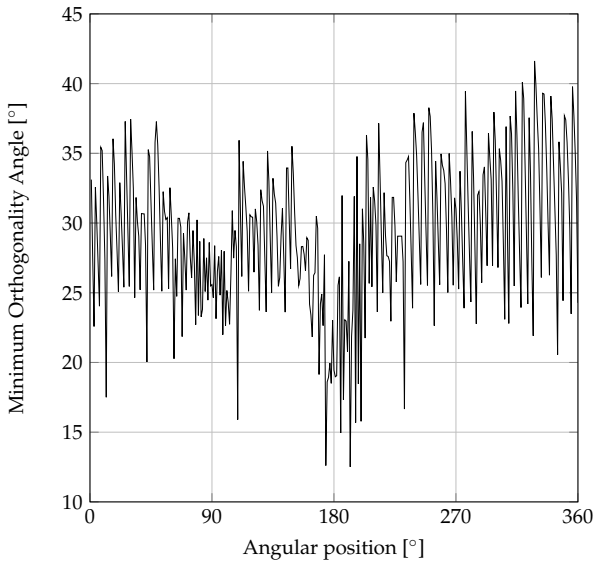

Figure 4: **Minimum orthogonality angle vs. angular position**

5. RESULTS AND DISCUSSIONS

Is this section we show the results that were obtained using the method previously described. Comparison with a simplified version of the analytical model presented by Mendoza *et al.* (2014) is made. The model uses equation 9 to predict power delivered by the device as a function of the following parameters: enthalpy h_{su} and specific volume v_{su} at inlet; enthalpy due to isentropic expansion $h_{iso,ex}$; exhaust pressure P_{ex}.

$$\dot{W} = \dot{m}_{in} \left[(h_{su} - h_{iso,ex}) + v_{su} \left(P_{iso} - P_{ex} \right) \right] \tag{9}$$

The total mass flow $\dot{m}_{total}$ is the sum of nominal mass flow $\dot{m}_{in}$ and mass flow in internal leakages $\dot{m}_{leak}$. The mass flow in internal leakages consider that Mach number reaches unity at leakages. Nominal mass flow is calculated from supply conditions (inlet) and swept volume rate. The details are given in Mendoza *et al.* (2014).

Pressure was monitored at inlet, outlet and selected positions of the domain during the CFD solution. The inlet pressure and outlet pressure are boundary condition, thus they assume constant values after the first revolution as shown in Fig. 5.

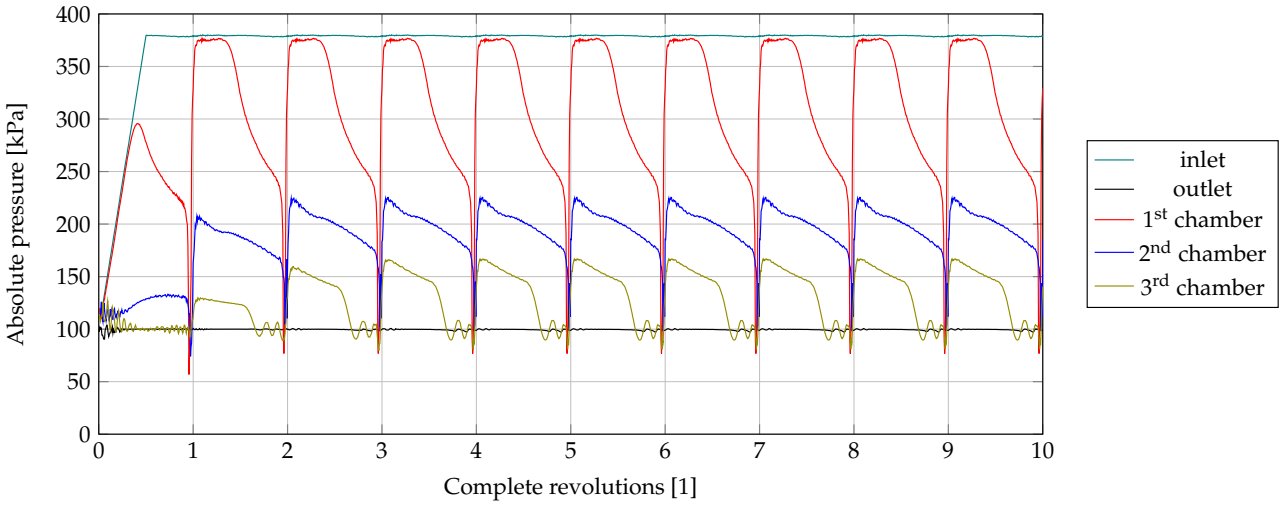

Figure 5: **Pressure evolution vs. angular position**

The pressure monitoring points for the chambers were placed at the center of the gap between the scrolls for θ=0°. This explains the abrupt pressure drop on angles close to 0°; this is caused due to the high velocity on the throat and, therefore, the local Mach number. As expected, there are 3 regions with uniform pressures. These regions are shown on Fig. 6 for θ angles of 0°, 90°, 180° and 270°. Connecting the curves from the three chambers it is possible to see the expansion process. At the very end it is possible to see a free expansion process, that characterizes under-expansion.

The under-expansion reduces the efficiency of the expander. The geometry considered in the current study should not present under-expansion with inlet and outlet pressures used as boundary conditions (see Tab. 2). We attribute this behavior to strong leakage caused by the $200\mu m$ flank gaps.

The power predicted by the analytical model, using Eq.9 is 1412 W. The power may be calculated with CFD simulation from the resultant torque imposed by the pressure distribution in the moving scroll walls. The power as a function of time is presented in Fig. 9. The averaged value for power was 823 W. We attribute this difference to stronger leakage than normal presented by the scroll with $200\mu m$ flank gaps. The experiment presented by Fanti *et al.* (2016), for the same geometrical configuration, reports peak power equal to 923 W at 2690 rpm, but at 2.94 bar at expander inlet. This different condition at inlet impedes a comparison with experiment.

Filling factor is defined at Lemort *et al.* (2009) as the ratio between the total mass flow rate passing through the machine and the mass flow rate theoretically displaced by the machine. Using the analytical model presented by Mendoza *et al.* (2014), the mass flow rate in the flank gaps may be calculated for the 200 μm flank gap and filling factor can be obtained, resulting in 1.94.

The CFD simulation allowed us to obtain filling factor as a function of time, as shown in Fig.8. The average value obtained with our numerical model was 1.63, what leads to a difference of 15.9% if compared to analytical model.

The throat velocity is shown on Fig. 7 for θ angles of 0°, 90°, 180° and 270°. The analytical model (Mendoza *et al.* (2014)) predicts 318.8 m/s. The flow between chambers is modeled analytically as a converging-diverging nozzle and only the velocity at the throat is relevant to predict mass flow between chambers. The CFD simulation reveals that the flow presents Mach number higher than one after the throat (diverging section) and returns to subsonic conditions after a shock.

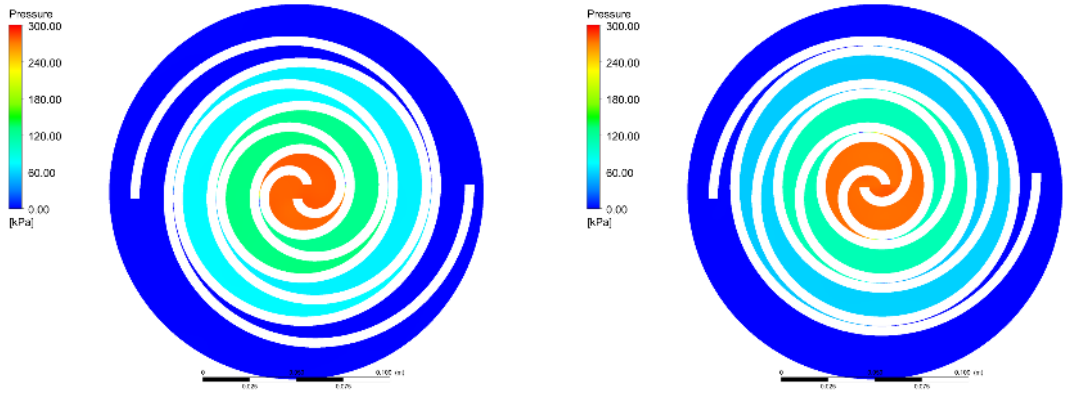

(a) θ=0° (b) θ=90°

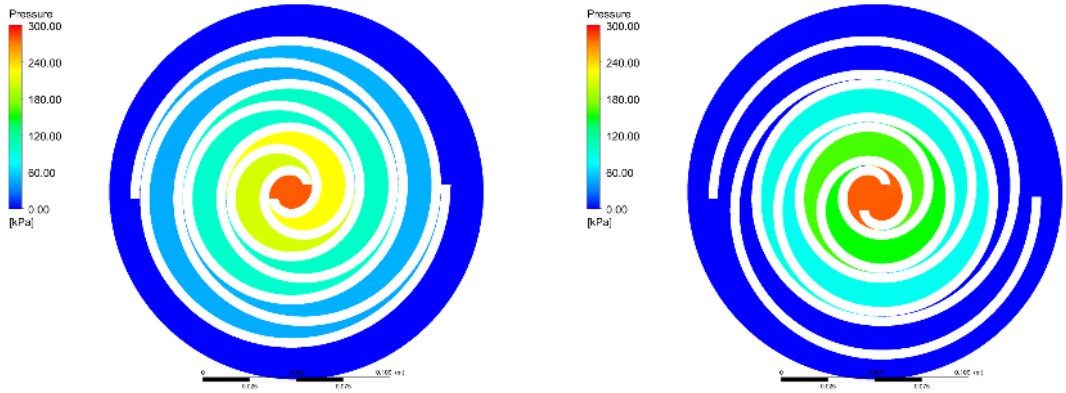

(c) θ=180° (d) θ=270°

Figure 6: **Pressure distribution**

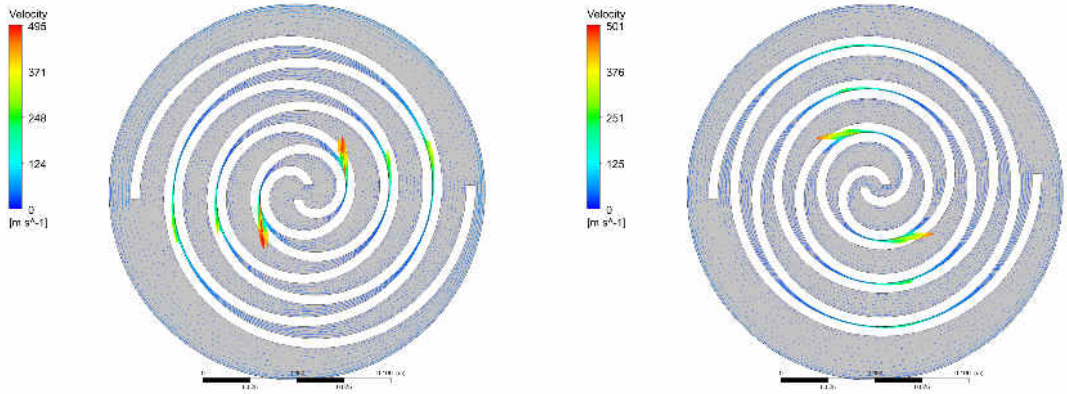

(a) θ=0° (b) θ=90°

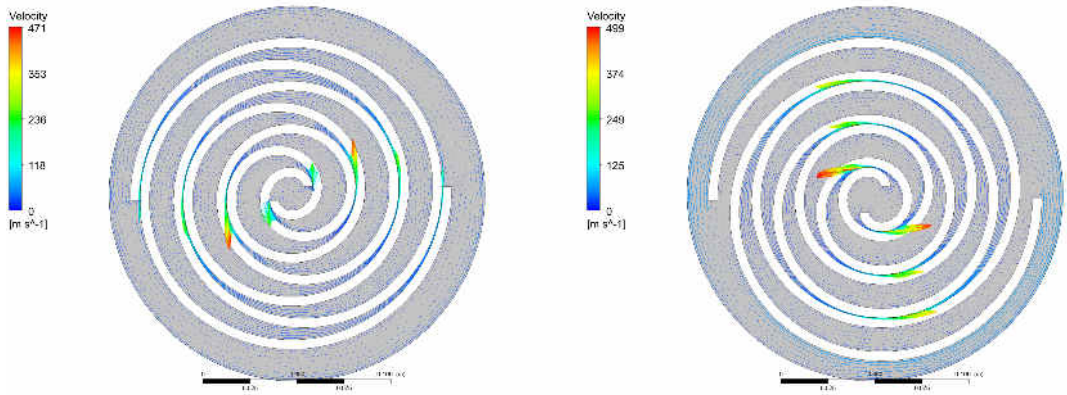

(c) θ=180° (d) θ=270°

Figure 7: **Velocity distribution**

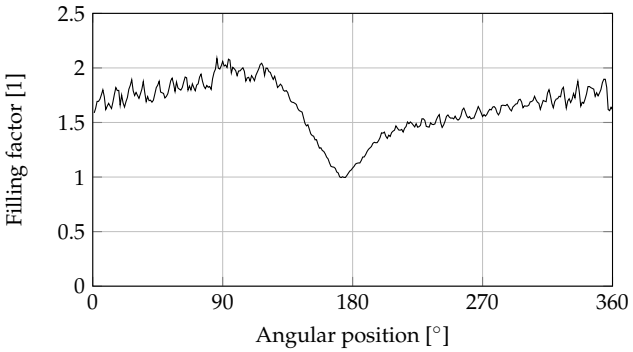

Figure 8: **Filling factor vs. angular position**

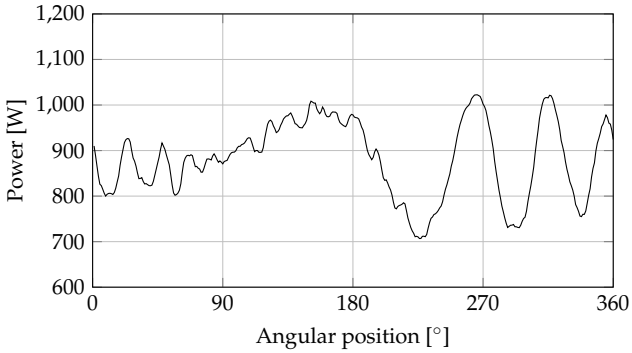

Figure 9: **Power vs. angular position**

6. CONCLUSIONS

In this work we presented a simulation strategy for the two dimensional CFD simulation of scroll expanders. The results obtained for power and filling factor are reasonably in good agreement with the analytical model predictions. More investigation should be conducted to compare simulation with results reported by Fanti *et al.* (2016).

7. ACKNOWLEDGEMENTS

The authors would like to acknowledge Centro Universitário da FEI and Fundação de Amparo à Pesquisa do Estado de São Paulo (FAPESP, Process No. 2011/17657-7) for the research support.

8. REFERENCES

ANSYS, C., 2016. "Release 17.0". *ANSYS CFX-Solver Theory Guide, ANSYS*.

Blunier, B., Cirrincione, G., Hervé, Y. and Miraoui, A., 2009. "A new analytical and dynamical model of a scroll compressor with experimental validation". *International Journal of Refrigeration*, Vol. 32, No. 5, pp. 874–891.

Declaye, S., Quoilin, S., Guillaume, L. and Lemort, V., 2013. "Experimental study on an open-drive scroll expander integrated into an orc (organic rankine cycle) system with r245fa as working fluid". *Energy*, Vol. 55, pp. 173–183.

Fanti, G.R., Donato, G.H.B. and de Mello, P.E.B., 2016. "A novel scroll expander for flank leakage investigation: preliminary tests". In *Proceedings of the 29th International Conference on Efficiency, Cost, Optimisation, Simulation and Environmental Impact of Energy System*.

Lemort, V., Quoilin, S., Cuevas, C. and Lebrun, J., 2009. "Testing and modeling a scroll expander integrated into an organic rankine cycle". *Applied Thermal Engineering*, Vol. 29, No. 14, pp. 3094–3102.

Mendoza, L.C., Navarro-Esbrí, J., Bruno, J.C., Lemort, V. and Coronas, A., 2014. "Characterization and modeling of a scroll expander with air and ammonia as working fluid". *Applied Thermal Engineering*, Vol. 70, No. 1, pp. 630–640.

Song, P., Wei, M., Shi, L., Danish, S.N. and Ma, C., 2015. "A review of scroll expanders for organic rankine cycle systems". *Applied Thermal Engineering*, Vol. 75, pp. 54–64.

Song, P., Wei, M., Shi, L. and Ma, C., 2013. "Numerical simulation of three-dimensional unsteady flow in a scroll expander applied in waste heat recovery". In *IOP Conference Series: Materials Science and Engineering*. IOP Publishing, Vol. 52, p. 042017.

Yanagisawa, T., Fukuta, M., Ogi, Y., Hikichi, T. *et al.*, 2001. "Performance of an oil-free scroll-type air expander". In *Proc. of the ImechE Conf. Trans. on compressors and their systems*. C591/027, pp. 167–174.

Zanelli, R. and Favrat, D., 1994. "Experimental investigation of a hermetic scroll expander-generator".

9. RESPONSIBILITY NOTICE

The authors are the only responsible for the printed material included in this paper.